Chemical Engineering & Processing: Process Intensification 202 (2024) 109838

Contents lists available at ScienceDirect

Chemical Engineering and Processing - Process Intensification

journal homepage: www.elsevier.com/locate/cep

# Solving the microwave heating uniformity conundrum for scalable high-temperature processes via a toroidal fluidised-bed reactor

Jose Rodriguez [a,*], Lorena Morona [a], Maria Erans [b], Adam J. Buttress [a], Matt Nicholls [a], Andrew R. Batchelor [a], Gabriela Duran-Jimenez [a], Sam Kingman [a], Daniel Groszek [c], Chris Dodds [a]

[a] Faculty of Engineering, University of Nottingham, NG7 2RD, United Kingdom
[b] Department of Chemical Engineering, ETSE, Universitat de València, Av. Universitat s/n, 46100 Burjassot-Valencia, Spain
[c] Torftech Technologies Ltd., 188 Greenham Business Park, RG19 6HW, United Kingdom

A R T I C L E I N F O

*Keywords:*
Microwave heating
Hybrid heating
Fluidised bed
High temperature
Thermal processing
Electromagnetic modelling

A B S T R A C T

Challenges exist to implementing high-temperature microwave processes with changing dielectric properties that achieve uniform processing. This paper presents a new high-temperature hybrid microwave processing system which overcomes these challenges in a robust, scalable way, integrating a slotted waveguide ring microwave feed into a toroidal fluidised bed reactor and maintaining its fluidisation behaviour. The prototype operates at a frequency of 2450 MHz with a maximum power of 10 kW and within a temperature range of 50–300 °C, though it is scalable to industrial levels. Electromagnetic simulations of the system were experimentally validated using a range of agri-crop feedstocks. Hydrodynamic and thermodynamic reactor characterisation was performed, and treatment performance was quantified regarding surface bed temperature variation. Excellent treatment uniformities were found under microwave and hybrid regimes, with a temperature coefficient of variation (CoV) across the bed's surface below 2 %, an order of magnitude better than existing microwave processes, generally regarded as highly uniform with CoV of approximately 20 %. The integration of microwaves and toroidal fluidised beds, without exposed moving parts, potentially unlocks a range of applications previously inaccessible to microwave technology or fluidised bed technologies on their own. Future work involves process development, techno-economic studies, and large-scale pilot trials.

## 1. Introduction

Microwave heating is a well-established technology used in the food and rubber processing industries for decades. However, these process temperatures are relatively low, typically under 150 °C. Developing microwave-based systems which operate reliably at temperatures higher than this presents significant challenges. These include but are not limited to: (1) appropriate construction materials, particularly for components exposed to high temperatures and electric field strengths, for example, microwave windows, seals, and ports. (2) Effective and reliable materials handling systems that can maintain performance over an acceptable period without costly and time-consuming maintenance regimes. For example, it is resistant to fouling and deposition of microwave-absorbing debris, which can lead to localised heating and system damage. (3) Reliable temperature measurement within the microwave applicator during operation and its' necessity to appropriately control microwave power delivery, particularly where this is automated into a wider process control regime. (4) Poor overall treatment uniformity impacting overall system performance and durability [1,2]. This poor uniformity can be a significant issue and may often be attributed to at least one or all the following factors:

- Changes in the strength of the electric field within the cavity and its subsequent interaction with the process material.
- A deficient material handling system or lack of mixing resulting in localised hot and cold spots; static and trapped material.
- Changing dielectric properties with temperature causes preferential heating, which can result in dielectric/thermal runaway, further exaggerating treatment heterogeneity.
- Localised process overheating and arcing.

Improvements in treatment homogeneity in a microwave process can be achieved in a number of ways. Movement of the material, e.g. by the use of turntables [3–5], non-uniform movement [6], conveying

* Corresponding author:
*E-mail address:* jose.rodriguez@nottingham.ac.uk (J. Rodriguez).

https://doi.org/10.1016/j.cep.2024.109838
Received 7 March 2024; Received in revised form 13 May 2024; Accepted 28 May 2024
Available online 29 May 2024

technologies [7–10], fluidised beds [11–14], and product mixing techniques [15,16]. Use of microwave susceptors [17–19]. Reactor geometry optimisation [20,21]. The movement of the electromagnetic fields, such as the use of mode stirrers [22,23], active reactor geometry modification [24], and microwave signal conditioning by frequency or phase sweeping [25–29]. The use of tailored microwave feeding configurations such as multiple feeds or feeding arrays optimised for a specific product [20,25,29–32]. Finally, optimise product size, shape, and positioning within the reactor [33–37]. Combining some of these principles can be a practical approach to optimising treatment uniformity and could be improved even further by combining microwaves with conventional heating technologies using a hybrid approach [38–40]. Most of these methods require complex moving parts, are inefficient, or poorly suited for use in high-temperature systems. They are often prone to debris accumulation, leading to overheating and the potential for thermal runaway, which can result in the burning or melting of components and insulation materials. It can also increase the likelihood of process arcing leading to critical system damage [41,42].

Fluidised-bed reactors are an established method of mixing materials during processing without moving parts for applications where mechanical means for product mixing or transport can become unpractical [43–45]. These reactors can be reliably operated at high temperatures, with industrial fluidised beds being used at temperatures in excess of 1000 °C [46,47].

By incorporating microwave heating in such fluidised beds, issues associated with microwave treatment uniformity and heat transfer limitations in processing low thermal conductivity solids can be reduced. Overcoming heat transfer limitations thanks to the volumetric heating effect of microwaves, which, when incorporated in a fluidised bed reactor, enables the processing of relatively large particles with highly efficient mixing of the material bed. Therefore, microwave integration can overcome a common constraint in conventional fluidised bed systems [12,48]. Moreover, combining external convection with internal volumetric heating could provide a high degree of control over the temperature gradient across the particles. Microwave fluidised beds have been investigated with an emphasis on drying applications, especially in food [14,49–57]. Other applications which have been explored include chemical reactions using metal powders [58], metal ores and concentrates [59,60] and recently, pyrolysis of biomasses [11,12,61]. These relatively simple systems are often derived from modified domestic ovens using a relatively microwave-transparent glass column acting as a fluidised bed reactor. Common issues with these systems arise from the fragile materials of construction, particularly the reactor tubes. The formation of char particles and microwave-absorbent by-products can easily stick to the inner surfaces of these tubes, making them prone to overheating and failure [62]. Exceptions can be found in the form of waveguides/ducts [13,49,50] and setups in which the fluidised reactor itself acts as a microwave cavity [59,63,64], and can provide more robust long-term operation.

In this paper, we present a hybrid convection-microwave heated fluidised bed system which combines both heating mechanisms to overcome uniformity and heat transfer limitations, resulting in a robust and scalable platform technology. This system is based on an established commercially available toroidal fluidised compact bed reactor (CBR) technology developed by Torftech® Ltd and the novel incorporation of microwave heating with minimal disruption of its fluidisation behaviour. Compared to a conventional fluidised bed, the CBR unit's advantages include high heat and mass transfer, rapid response to process control, low static pressure loss (i.e. ease of high-temperature gas recirculation), and tolerance to feed size variability [65]. Adapting the design has enabled the integration of a microwave applicator, which maintains the characteristic hydrodynamic behaviour and represents a viable and scalable route to reliable high-temperature microwave processing, offering a highly uniform heating, controllable temperature gradient across the product, relatively large particle size, and rapid processing. The design is hereby referred to within this work as the Torwave® hybrid microwave system and is conceptually illustrated in Fig. 1. The design approach, modelling, experimental validation and characterisation are presented for a one-litre batch proof of concept system. The system could find applicability in sustainable processes, such as process intensification, carbon capture, torrefaction, exfoliation, roasting, sterilisation, expansion, drying, reduction, amongst many others.

## 2. Integration of a toroidal fluidised bed and microwave applicator - Design Approach

A microwave design frequency of 2450 MHz of the Industrial Scientific and Medical (ISM) bands was selected as a principal basis of design parameters for the prototype proof-of-concept system. The dimensions of a resonant microwave reactor are generally bound by the frequency of the microwave energy and its resonant behaviour (i.e. mode patterns). This, in turn, is dependant on the geometry of the cavity itself [45]. The use of a 2450 MHz prototype yields a system of acceptable size, which serves as an appropriate platform for proof-of-concept development and performance evaluation whilst also being large enough so that the reactor design scale-up is well understood. Any subsequent scale-up approach would primarily be based on reducing the operational frequency to the 896 MHz band in the UK or 915 MHz internationally, with its relative reactor and bed size increase. CBR reactors can also be scaled in diameter, maintaining the bed cross-section shape and enabling scale-up at a fixed frequency by redesigning the microwave feeding structure. In the following sections, we present the general arrangement of the reactor, its Basis of Design (BoD) and the electromagnetic design of the integrated microwave applicator system.

### *2.1. General arrangement of the proof-of-concept torwave® T400 reactor*

The Torwave® is characterised by a quasi-triangular cross-section toroidal bed formed between the internal cone and the outer wall of the reactor. This bed covers approximately 95 % of the blade distributor [66]. The system has the capacity to operate with volumes of up to one litre per batch, depending on the particle size. The bed density can be relatively high, with a void fraction of 0.39 achievable for regular spherical particles [67], closely resembling the expected void fraction from a poured random packing model for spherical particles [68]. The design incorporates a 60 ° pitch truncated cone and a 4 cm distributor blade ring. The layout of the proof-of-concept laboratory scale system and the reactor's main components are depicted in Fig. 2.

A 4 kW fan delivers air to a 10 kW in-line electrical heater directly connected to the reactor plenum. The recirculation loop, connecting the reactor outlet to the fan, is made of stainless-steel circular ducting. The reactor and the recirculation loop are insulated using aluminium-coated glass fibre insulation. The process gas temperatures were monitored using three K-type thermocouples at the fan outlet, reactor inlet, and reactor outlet. The bed temperature was measured across the moving bed using a thermal camera (FLIR 60E) fixed above a viewing port in the lid fitted with a Germanium window, which consists of a metal tube sized to prevent microwave leakage, following a similar design approach as in [69]. A WR284 waveguide feeds microwaves to the slot waveguide ring, which distributes the microwaves uniformly around the reactor chamber base through a microwave transparent window, which is conformal to the reactor distribution cone.

### *2.2. Basis of design*

The basis of design specification summary can be found in Table 1, for a pilot-scale and laboratory-scale system.

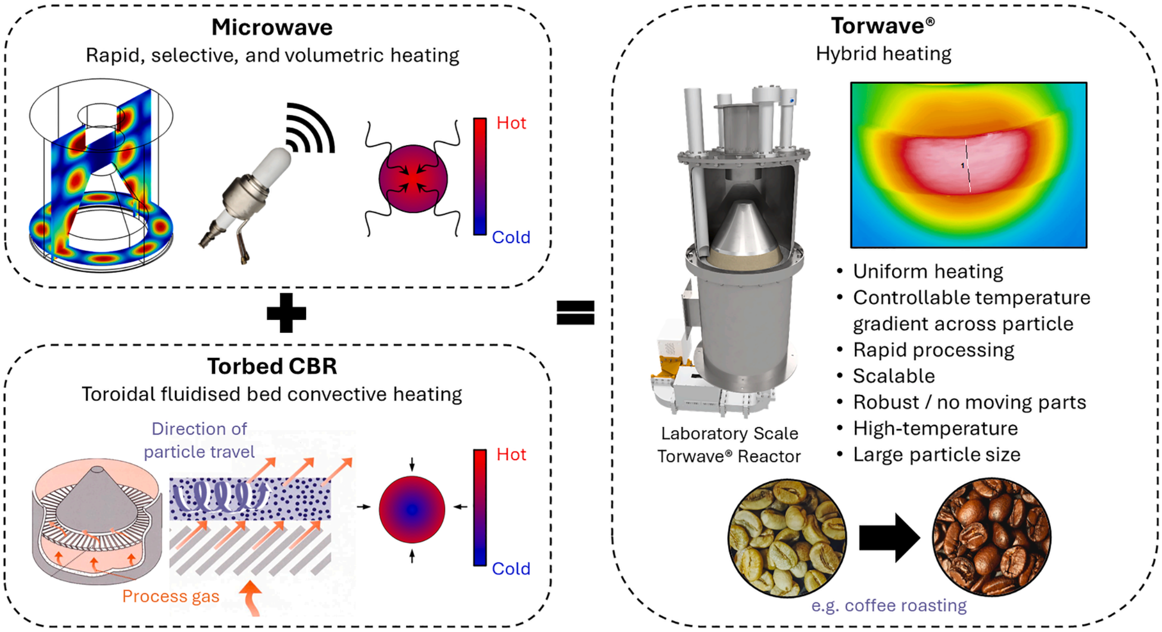


**Fig. 1.** Illustration of the Torwave® reactor concept.

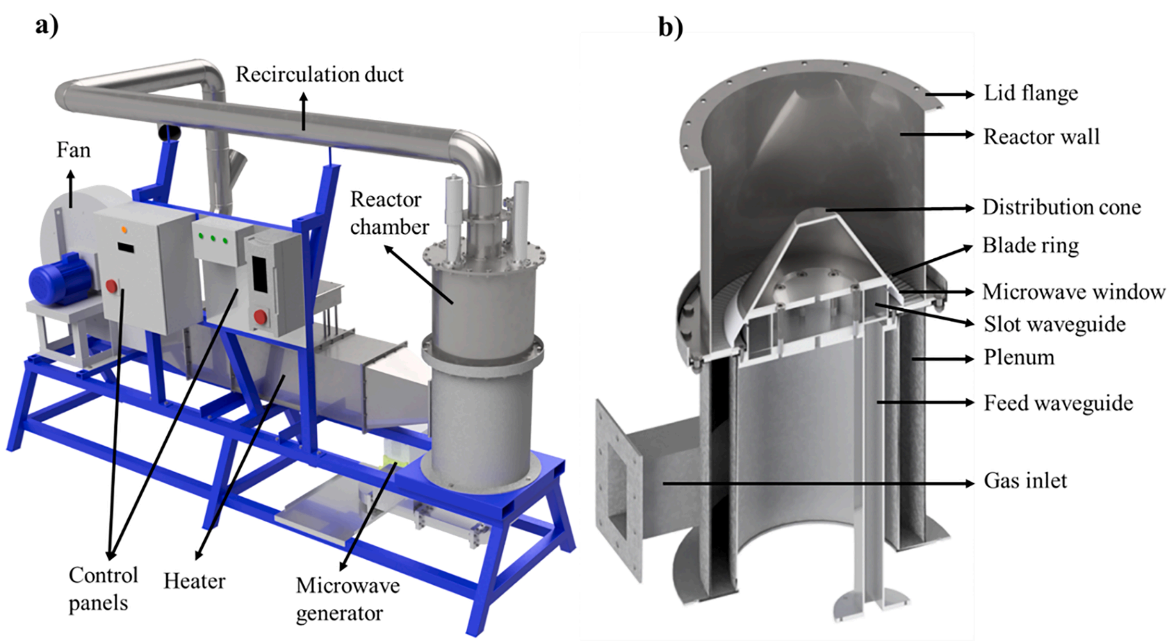


**Fig. 2.** Illustration of Torwave ® T400 proof of concept laboratory system showing the general arrangement of the unit (left) and internal reactor geometry (right).

### *2.3. Electromagnetic modelling methodology*

The resonant properties of the CBR reactor were characterised through electromagnetic simulation. Also, a compatible microwave feeding concept was developed, which does not interfere with the hydrodynamic function of the system, delivers an even distribution of power across the bed, and achieves the BoD design requirements regarding power conversion efficiency, power density and leakage. The design process relied on COMSOL Multiphysics RF module based on the finite element method (FEM) [70]. The geometry was discretised with a maximum element size of $\lambda/5$ in the bulk and $\lambda/10$ within the bed volume, where $\lambda$ represents the wavelength inside of the material (i.e. $\lambda = \lambda_0/\sqrt{\varepsilon_r'}$, with $\lambda_0$ being the free-space wavelength and $\varepsilon_r'$ the dielectric constant of the material).

Isotropic media with bulk properties derived from experimental measurements were used to model the products. Metallic surfaces were approximated as impedance boundaries due to the significantly smaller skin depth compared to any metallisation present in the system. This approximation assumes that the currents are superficial, which can be considered accurate if the ratio of metallisation dimension (L) to skin depth ($\delta$) is greater than 10 [70]. The skin depth can be calculated using Eq. (1) [71].

$$\delta = \sqrt{\frac{1}{\pi f \mu_0 \mu_r \sigma}} \tag{1}$$

where f is the frequency (Hz); $\mu_0$ is the permeability of free space (H/m) and $\mu_r$ are the relative permeability (H/m) and σ is conductivity (S/m).

**Table 1**
Basis of design – summary of requirements.

| Parameter | Aspect | Requirement (Pilot-scale) | Requirement (Proof-of-Concept scale) |
|---|---|---|---|
| Scope and operation | Operation mode | Semi batch-mode | Batch-mode |
| | Capacity | 16 Litres per batch | 0.5–1 Litres (per batch) |
| | Service & Operability | Fully dismountable and serviceable | Fully dismountable and serviceable |
| | Bed temperature | Up to 800 °C (subject to material specification) | Up to 300 °C (subject to material specification) |
| Microwave system | Power | 75 to 100 kW | 1 to 10 kW |
| | Frequency | 896 or 915 MHz | 2450 MHz |
| | Efficiency | > 90 % Power absorbed | > 90 % Power absorbed |
| | Average power density in the load | Up to ~1 × $10^7$ W/$m^3$ | Up to ~1 × $10^7$ W/$m^3$ |
| | Health and safety compliance | Leakage below 5 mW/$cm^2$ | Leakage below 5 mW/$cm^2$ |
| Fluidised bed | Diameter | 1000 mm | 400 mm |
| | Gas temperature | 25 °C to 800 °C | 25 °C to 300 °C |
| | Operational mode | Recirculating (w/ cyclone) | Recirculating |
| Products | Particle size range | 1–18 mm | 1–9 mm |
| | Bulk density | Up to 1 g/$cm^3$ | Up to 1 g/$cm^3$ |

The electromagnetic wave equations for the electric fields (E) are solved in the frequency domain, following Eq. (2) [70].

$$\nabla \times \frac{1}{\mu_r}(\nabla \times E) - \omega^2 \varepsilon_0 \mu 0 \left(\varepsilon_r - \frac{j\sigma}{\omega \varepsilon_0}\right) E = 0 \quad (2)$$

### 2.4. Additional metrics

A number of additional metrics were employed to assess the electromagnetic performance of the system. The average power density within the volume V is determined using Eq. (3).

$$P_{davg} = \frac{1}{V}\int_V P_d dV \quad (3)$$

where $P_d$ is the power density ($Wm^{-3}$), V is the bed volume ($m^3$)

This value enables evaluating the likely power density achievable within the process material for a given input microwave energy. Experimental determination is difficult, except in cases where most of the absorbed power is anticipated to be dissipated in the product. In such scenarios, an estimation can be done by calculating the ratio of dissipated power to sample volume.

To evaluate the uniformity of microwave distribution within a volume, the Power Uniformity Index (PUI) is used. This index is determined by averaging the spread of power density data and normalising it to the average power density. The calculation of the PUI can be performed using Eq. 6 [72]:

$$PUI = \frac{\int_V \sqrt{(P_d - P_{davg})^2} dV}{V\ P_{davg}} \quad (4)$$

The minimum achievable PUI is zero for a perfectly uniform power density distribution throughout the product (i.e., the power density evaluated in each point within the volume is equal).

### 2.5. Torwave® resonant behaviour

A simplified T400 CBR reactor geometry with a diameter of 400 mm (hence T400), as depicted in Fig. 3, was subjected to an eigenfrequency study. This analysis aimed to investigate the resonant behaviour of the cavity and identify appropriate resonant modes for heating the material in the fluidised bed.

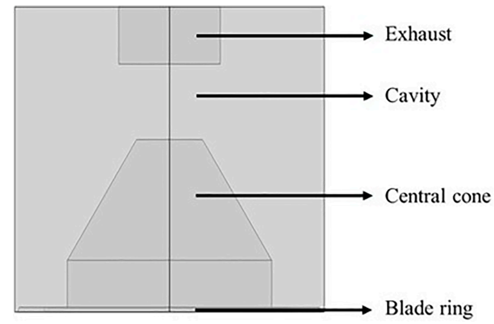


**Fig. 3.** Reactor simplified geometry for eigenfrequency analysis.

From the various resonant modes available within the cavity, a specific mode exhibited the greatest degree of interaction with the load upon establishing the fluidised bed, with a relatively high empty quality factor ($Q_0$) of 8329. This mode is illustrated in Fig. 4, showing the presence of eight vertically polarised hotspots within the product bed zone.

The quality factor ($Q_0$) is defined as [44]:

$$Q_0 = \frac{2\pi U}{P} \quad (5)$$

where: U total energy stored and P the energy dissipated per cycle.

To attain high power conversion efficiencies, it is essential to have a high quality factor for an empty reactor ($Q_{0empty}$) and a low quality factor with a reactor with product ($Q_{0filled}$). The power conversion efficiency refers to the proportion of absorbed power within the system that is dissipated within the product. It can be calculated as shown in Eq. 6 [73]:

$$P_{eff}\ (\%) = \left(1 - \frac{Q_{0filled}}{Q_{0empty}}\right) \times 100 \quad (6)$$

### 2.6. Slot ring feed design

To achieve the design resonant behaviour, it was necessary to establish a means of transferring energy to the load and thus to the resonant pattern. Ideally, this mechanism would not interfere with the gas flow in the reactor or the fluidised bed's hydrodynamic characteristics. Importantly, the toroidal and roping motion of the bed causes frequent collisions between the product and the outer reactor wall, while the central cone seldom comes into contact with the product.

A novel concept comprising a slot waveguide array that conforms to a conically shaped microwave transparent window on the central cone

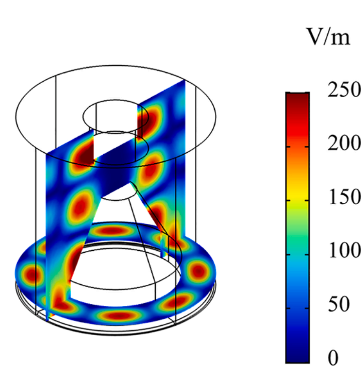


**Fig. 4.** Electric field distribution resonant mode at 2541 MHz for the empty cavity. Vertical cut plane at the centre, and horizontal cut plane at expected bed position.

was designed. This array enabled close coupling with the product in a predominantly vertically polarised field, ensuring efficient microwave energy delivery to the product bed. Combined with the excellent bed mixing characteristics of the CBR reactors, it can facilitate uniform microwave treatment of the product bed. By positioning the microwave window in a low position conformal to the base of the central cone, the concept minimises the risks of wear and contamination during prolonged operation as the material only has limited physical contact with the central cone. Additionally, power can be evenly distributed throughout the reactor chamber, aligning with the resonant pattern of the cavity. This minimises the likelihood of reduced treatment uniformity and process stability issues such as overheating and arcing, which can be expected in less controlled feeding arrangements.

### 2.6.1. Slot waveguide design

Slotted waveguides have been widely employed as antenna arrays [74–79]. These waveguides feature slots that disrupt the current flow, causing it to circumvent the slots and radiate as an equivalent half-wave dipole. Broad wall slot antennas generate vertically polarised fields, while narrow wall slots produce horizontally polarised fields [79]. Moreover, slots can be utilised to couple fields from a waveguide to a product or cavity, enabling controlled material processing [45,44,80]. In this context, such a coupling structure can effectively couple microwaves to the cavity.

For effective propagation of electromagnetic energy into the wider cavity, the longer side of a slot should be orientated perpendicular to the current to disrupt its flow effectively. In the travelling wave regime, the current maximum shifts with the wave, while in the standing wave regime, the maxima become fixed and spaced apart by $\lambda_g/2$, where $\lambda_g$ represents the guided wavelength. Fig. 5 illustrates the surface current for two slots on the broad side of a $TE_{10}$ waveguide. It demonstrates that a slot positioned in the middle of the broad side with its long side parallel to the waveguide walls would not exhibit significant radiation, whereas an off-centred slot would.

The resonant length of a slot, which behaves complementary to a half-wave dipole, is typically around $\lambda_0/2$, considering a finite slot width of approximately $0.035\lambda_0$. In practice, the slot length is usually around $L_c \approx 0.4625\lambda_0$ [78,81].

## 2.7. Ring-shaped array

A H-tee power splitter concept was used to realise the ring-shaped waveguide slot array, where the output arms of the splitter are in phase (Fig. 6). Closing the ring with equal-length arms results in a maximum electric field opposite to the input, as the waves meet in phase and constructively add at the joint (i.e., virtual open circuit).

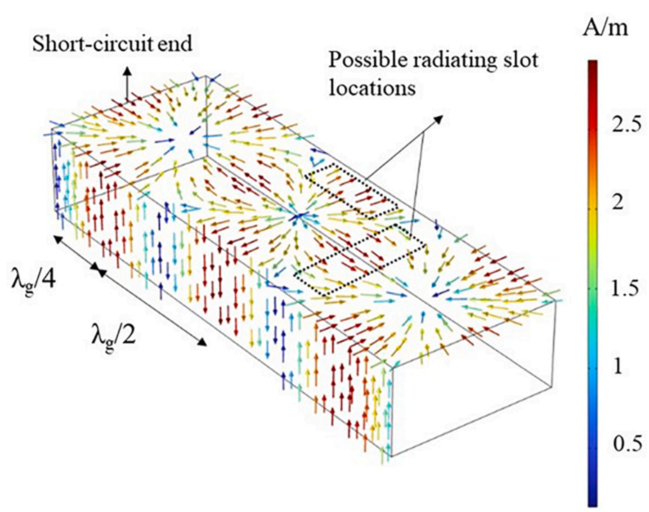


**Fig. 5.** $TE_{10}$ rectangular waveguide surface current distribution schematic representation for different slot positions.

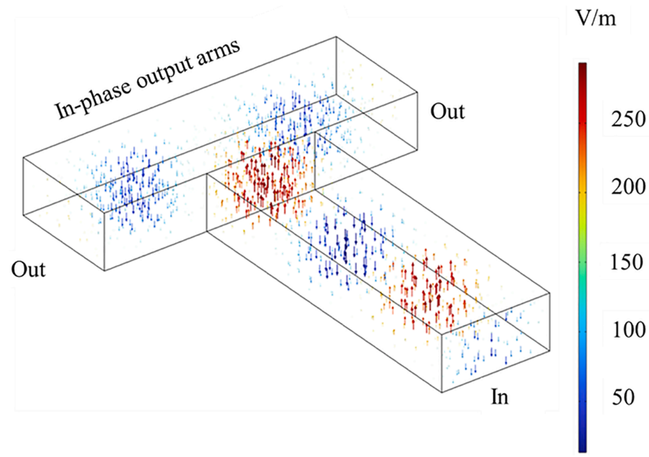


**Fig. 6.** H tee splitter electric field behaviour representation for a fix input phase, blue arrows electric field vector pointing down, red arrows pointing up, showing output arms in phase.

This behaviour is illustrated in Fig. 7, which depicts the electric field across the centre of the ring.

The ring array was dimensioned to present eight maxima aligned with the identified reactor resonant mode hot spots shown in Fig. 4. A maximum occurs opposite the feed, with subsequent maxima separated by half the guided wavelength. When the waveguide is bent into a ring shape, this distance needs to be measured along the internal circumference. Given a guided wavelength of $\lambda_g$=173.6 mm, the half wavelength, representing the arc length between the slots, is $R\theta = \lambda_g/2$, leading to an approximate angular separation of $\theta \approx 46^\circ$. A last combined maxima is located at the feeding point, resulting from the superposition of two slightly displaced maxima extending along each arm, resulting in a total of eight zones that align with the reactor resonant mode.

The vertical position of the slot in the waveguide wall influences the coupling efficiency. Slots positioned further from the centre exhibited a greater degree of individual coupling. Therefore, careful consideration of this position was required to achieve efficient and uniform distribution around the ring considering the range of dielectric properties of the materials considered in the electromagnetic design.

In antenna arrays, subsequent slots are typically interleaved in opposite positions to minimise the horizontally polarised component in the far-field [79]. However, this is not a requirement for heating

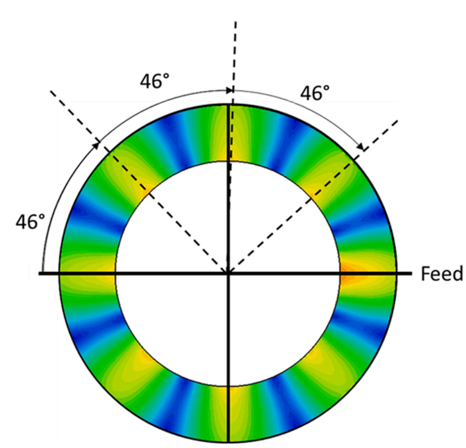


**Fig. 7.** Electric field distribution within the waveguide ring at its centre, designed for broad wall slot feeding.

purposes and near-field operation. To optimise the feeding ring within the boundary constraints of the reactor, the slots were located only at the upper end of the waveguide, and the ring position was numerically optimised to achieve at least half power coupling without tuning for beds with dielectric constants (ε') ranging from 1.5 to 3 and a loss factor (ε") of 0.08 (representing the lower end of the loss factor for materials processed in the system). This optimisation allows for reasonable ease of system tuning. The evaluation of key performance parameters for different product properties under untuned conditions is presented in Table 2 and shows that the system is robust enough to operate in the expected range of material properties, as target BoD parameters were achieved in all cases.

## 3. Selected materials and their dielectric properties

In order to validate the reactor's field and power density distribution and its resonant properties, electromagnetic simulations were conducted using a lightweight foamed glass incorporating a small proportion of carbon powder (FOAMGLAS T4+). This material is considered an excellent microwave absorber as the foamed structure retains heat with minimal thermal conduction through the material.

One of the most important considerations for fluidised process is to ensure flow regime is maintained. In this sense, the impact of bed loading (0.5 – 1 L), particle size (1- 9 mm), temperature (25 – 300 °C) and gas flow rate was systematically investigated to evaluate the toroidal fluidised regime. The dynamic testing validation was performed using a range of materials such as green coffee beans, mung beans, mustard seeds and malted barley. The selection of these materials was done based on the physicochemical and mechanical properties, including moisture, particle size, density and morphology. These samples were also used to characterise thermodynamic, heating uniformity and resonant characteristics of Torwave®.

Dielectric property measurements were performed using the cavity perturbation technique (CPT) [82] at 2470 MHz on FOAMGLAS® T4+, Polytetrafluoroethylene (PTFE), green coffee beans, mung beans, mustard seeds, and malted barley, with results shown in Fig. 8. Samples were run in triplicate, and the figures reported the average values.

As a function of temperature, the dielectric properties of FOAMGLAS T4+ remain relatively constant, making it an ideal candidate for its use for static validation with thermal imaging. PTFE exhibited a negligible loss factor across the measured range of material temperatures and was measured as a low-loss comparator.

Considering the dielectric response of coffee and mung beans, both the constant (ε') and loss (ε") increase up to a maximum reached 140 – 150 °C and are associated with their softening point. After this temperature, relatively abrupt drops in both properties are observed, resulting principally from water loss and the devolatilisation of aroma compounds. Materials can be classified according to their ability to absorb microwaves [83]. Green coffee beans can be classed as moderate to strongly microwave-absorbing materials, having a loss tangent (ratio of ε''/ε') from 0.08 to 0.15 over the measured temperature range. Mung beans can be classed as strong microwave absorbing as their loss tangent is within the 0.12–0.15 range.

**Table 2**
Performance of a reactor at 2.45 GHz, for a 6 kW microwave power input at a range of bed dielectric constants and a loss factor of 0.08 (untuned condition).

| Parameter | $\varepsilon' = 1.5$ | $\varepsilon' = 2.0$ | $\varepsilon' = 2.5$ | $\varepsilon' = 3.0$ |
|---|---|---|---|---|
| S11 (dB) | −4.4 | −4.7 | −3.1 | −10.3 |
| Peff (%) | 90.3 | 88.3 | 88.2 | 82.7 |
| PUI | 0.83 | 0.70 | 0.85 | 0.84 |
| Pav (W/m3) | $3.75 \times 10^6$ | $3.82 \times 10^6$ | $2.88 \times 10^6$ | $4.93 \times 10^6$ |

Where: $S_{11}$ is the reflection coefficient magnitude; $P_{eff}$ (%) is power conversion efficiency; PUI is the Power Uniformity Index and Pav is average power density in the load.

The dielectric properties of malted barley increase proportionally up to 250 °C. Again, as with coffee and mung beans, the dielectric response up to 150 °C is principally dominated by the interaction with free water within the cereal grain. However, above this temperature, the interaction with bound water associated with β-glucans, phenolic compounds, and structural carbohydrates dominates [84]. Having a loss tangent in the rage 0.04–0.08 malted barley was classed as a moderate microwave absorber.

Considering the mustard seeds, the dielectric properties increase slightly with temperature, up to 100 °C and drop up to 250 °C. However, the variance is significantly less than the other materials tested. Loss tangent for the mustard seeds was ~0.04 over the temperature measurement range, thereby classed as a moderate microwave absorber.

Further dielectric measurements were done using a WR430 waveguide transmission-reflection dielectric measurement system [85]. This system allows the measurement of bulk dielectric properties of malted barley without grinding, as is required for CPT; thereby, it is expected to yield results more representative of the material introduced to the Torwave® reactor during processing. Results at 20 °C show a dielectric constant ε' of 2.08 and loss ε" 0.18 when measured at 2470 MHz. This is similar to the values derived from the CPT indicating that grinding has little effect on measured dielectric properties compared to the whole grain.

## 4. Experimental characterisation and validation

### 4.1. Static validation

To validate the heating pattern and resonant characteristics (i.e. reflection coefficient $S_{11}$) of the reactor against electromagnetic simulation, the FOAMGLAS® T4+ described in the previous section was cut to mimic a typical bed shape during normal operation in the Torwave reactor, with the shape shown in Fig. 9.

The foam ring was supported by a 5 mm tall microwave transparent ceramic fibre blanket placed on the distributor blades. The reflection coefficient of the system was measured using a Keysight E5071C vector network analyser connected to the system's waveguide input.

Fig. 10 shows the simulated vs. measured reflection coefficient ($S_{11}$) in dB, which represents the fraction of the microwave power being input to the reactor being reflected to the generator ($P_{reflected} = P_{in}\left(10^{\frac{S_{11}}{10}}\right)$). Across the frequency range, measurements show close agreement with the $S_{11}$ output from the simulation, typically, with a −10 dB bandwidth difference of about 1 MHz. The close correlation underpins the simulation method's suitability to evaluate the reactor's behaviour.

During the static heating tests, the FOAMGLAS® T4+ ring was exposed to an applied microwave power of 300 W for 10 s. The reactor lid was promptly removed, and a thermal image of the entire bed was captured by looking down into the reactor from above using a NEC H2640 infrared thermal camera. Images were then analysed using Radiometric Complete® software. The resulting thermal distribution profiles were qualitatively compared to a 2-dimensional simulated power density distribution taken from the same reactor area – just above the blade distributor where the fluidised bed is formed. Fig. 11 shows the simulated power loss density and the measurements obtained from the thermal image. These results agree with the spatial distribution of the electric field intensity and heating pattern observed on the surface of the material. This further validates the electromagnetic design approach.

### 4.2. Hydrodynamic characterisation

To better understand the system's fluidisation behaviour and simulate the fluidised bed, the stainless-steel chamber shown in Fig. 1 was replaced with an optically transparent Perspex chamber. The Perspex chamber enabled clear observation of bed dynamics and characterisation of the system's fluidisation behaviour.

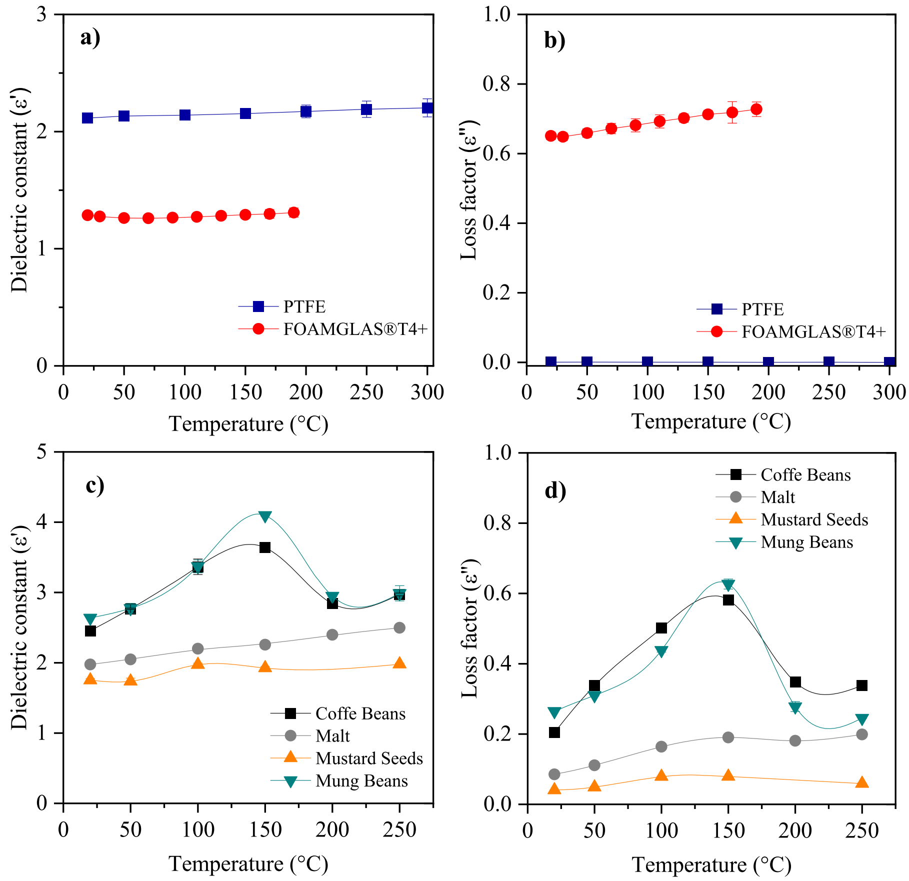


**Fig. 8.** Dielectric constant (a) and loss factor (b) versus temperature of PTFE and FOAMGLAS®T4+ and Dielectric constant (c) and loss factor (d) for different materials at 2470 MHz– Average of three measurements measured by CPT.

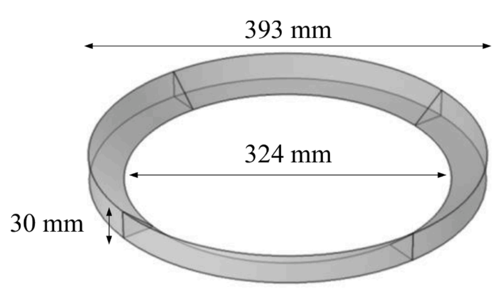


**Fig. 9.** Sketch of static bed, representing a typical bed shape obtained in the CBR reactor.

The materials selected to evaluate the hydrodynamic behaviour are shown in Table 3. These materials allowed to evaluate the toroidal fluidisation using a range of samples with industrial relevance and characterised by their unique characteristics such as particle sizes, shapes, densities, and classification based on Geldart's particle classification system.

The samples were fluidised using three different volumes to explore different bed loading configurations (200, 400, and 600 mL). The bed pressure drop was measured at various gas velocities for each fluidisation regime. The relationship between bed pressure drop and gas velocity is illustrated in Fig. 12, providing a typical variation observed in the described fluidisation regimes.

Observations of the bed during toroidal fluidisation were undertaken using a high-speed camera. A minimum load volume was required to achieve toroidal fluidisation of some particle types, and glass pebbles were not toroidally fluidisable above 600 mL with the used fan due to their density. The required velocity ranges to achieve toroidal fluidisation are shown in Table 3. For stable operation, a velocity near the midpoint between minimum and maximum was used during processing runs.

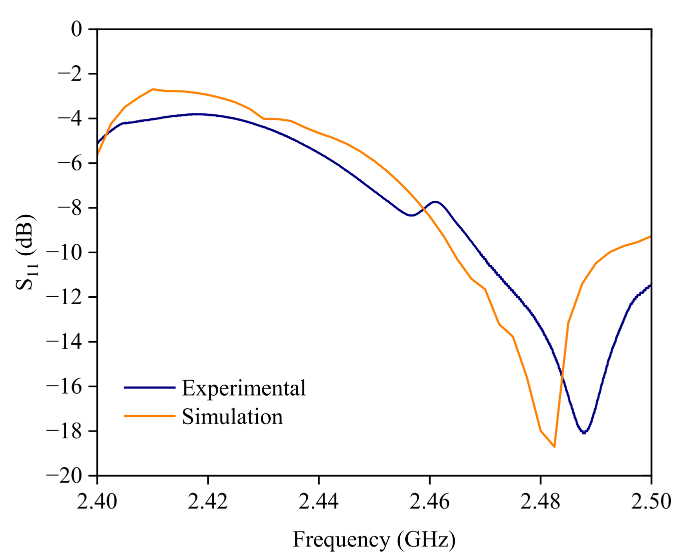


**Fig. 10.** Experimental (blue line) and simulated (orange line) reflection coefficient with FOAMGLAS®T4+ ring as load inside the reactor.

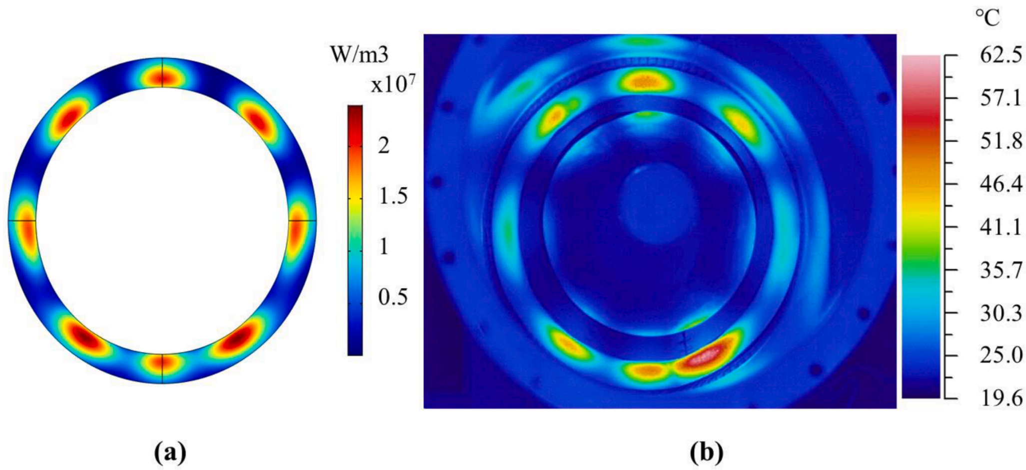


**Fig. 11.** Simulation of power density distribution at the bed surface using FOAMGLAS ®T4+ (a) compared to a static heating test using the same material (b).

**Table 3**
Hydrodynamic characterisation of different particles for toroidal fluidisation.

| Particle | True density (g/L) | Bulk density (g/L) | Size (mm) | Sphericity | Geldart's Classif. | $U_{mft}$-$U_{maxft}$ 200 mL (m/s) | $U_{mft}$-$U_{maxft}$ 400 mL (m/s) | $U_{mft}$-$U_{maxft}$ 600 mL (m/s) |
|---|---|---|---|---|---|---|---|---|
| Quinoa | 1393.2 ± 2.2 | 757 ± 3 | 2.5 | 0.76–0.78 | B | 2.16–4.85 | 3.01–5.44 | 3.54–6.17 |
| Corn | 1404.8 ± 0.2 | 867 ± 2 | 4–5 | 0.67–0.69 | D | – | – | 5.51–5.97 |
| Mustard Seeds | 1105.0 ± 0.1 | 717 ± 2 | 2–2.5 | 0.87–0.89 | D | 2.43–4.21 | 2.49–4.83 | 3.34–5.31 |
| Marrowfat peas | 1407.5 ± 0.6 | 833 ± 6 | 8–9 | 0.89–0.91 | D | – | – | 5.84-N/A |
| Couscous | 1435.4 ± 0.1 | 776 ± 4 | 2–2.5 | 0.82–0.84 | B | 2.36–4.13 | 2.42–4.79 | 2.95–5.31 |
| Plastic beads | 929.7 ± 0.2 | 855 ± 3 | 4.5 | 0.76–0.78 | D | 2.75–3.54 | 3.15–4.33 | 3.94–6.63 |
| Mung beans | 1386.6 ± 0.2 | 869 ± 3 | 5–6 | 0.84–0.86 | D | – | – | 5.51–6.96 |
| Malted barley | 1406.1 ± 1.0 | 558 ± 3 | 8.5–9 | 0.53–0.55 | D | – | 2.75–4.59 | 3.48–6.57 |
| Coffee beans | 1312.6 ± 0.4 | 618 ± 3 | 8–9 | 0.68–0.70 | D | – | 4.01-N/A | 5.18–6.82 |
| Glass pebbles | 2527.1 ± 0.3 | 562 ± 3 | 2 | 0.63–0.65 | D | – | 5.65–7.18 | N/A |

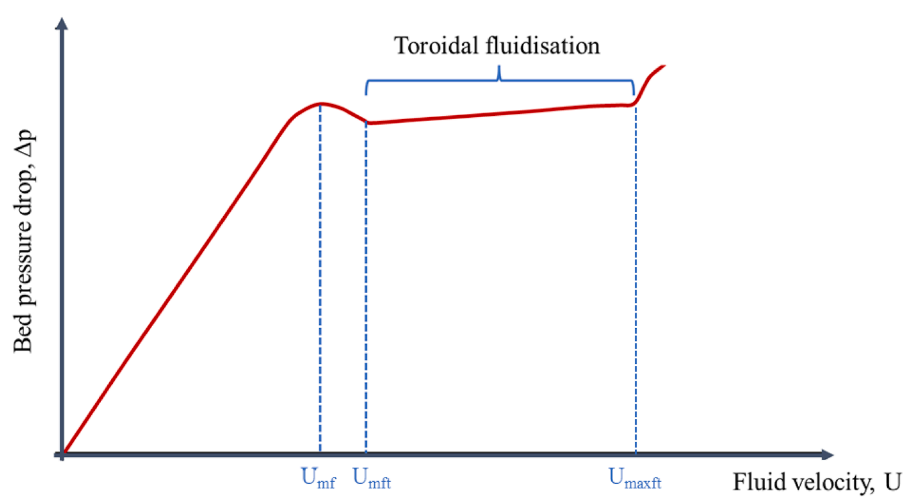


**Fig. 12.** Pressure drop vs. gas velocity in a TORBED reactor ($U_{mf}$ – minimum fluidisation velocity, $U_{mft}$ - toroidal minimum fluidisation velocity), adapted from [86].

### 4.3. Dynamic validation

To compare the electromagnetic simulations with experimental behaviour with a moving bed, measurements of the physical shape of a malt fluidised bed were taken to estimate the fluidised volume and fluidised bed density for two load volumes of 500 ml and 600 ml, respectively. An estimation of the fluidised bed bulk dielectric properties was performed using the Complex Refractive Index (CRI) mixing rule to estimate properties at fluidised density from the measured properties [87]

$$\varepsilon_b = \sqrt{\left(\sqrt{\varepsilon_a} - 1\right)\frac{\rho_b}{\rho_a} + 1} \quad (7)$$

where $\varepsilon_b$ is the estimated complex relative permittivity of at a $\rho_b$ (g/L) density (fluidised bed density), $\varepsilon_a$ is the measured complex relative permittivity, measured at a $\rho_a$ (g/L) density.

The observed fluidised bed densities and estimated bulk dielectric properties of the fluidised bed is shown in Table 4.

**Table 4**
Observed fluidised bed densities and estimations of the respective fluidised bed bulk dielectric properties for malted barley samples.

| Sample type | Sample size (mL) | Fluidised density $\rho_b$(g/L) | Density ratio $\rho_b/\rho_a$ | $\varepsilon_b$ |
|---|---|---|---|---|
| Malt | 500 | 296.4 | 0.52 | 1.5-j0.08 |
| Malt | 600 | 363.2 | 0.63 | 1.64-j0.10 |

Reflection coefficients were measured using a Keysight E5071C vector network analyser connected to the waveguide input via a coaxial to waveguide transition. The system was tuned using a 3-stub tuner to achieve resonance at 2.45 GHz. Simulations were done using the observed bed shape and estimated fluidised bed dielectric properties, and tuned for resonance at 2.45 GHz. The results are shown in Fig. 13.

Both experimental and simulation results demonstrate good agreement regarding the main resonance at 2.45 GHz with virtually the same half-power bandwidth. Therefore, the results obtained from the model are deemed suitable for estimating the system's response and evaluating its performance for materials, provided dielectric properties and fluidisation characteristics are known. It also underpins its use as a valuable tool for design and scale-up investigations. Furthermore, similar responses are obtained across the range of bed volumes evaluated and well within BoD power delivery requirements.

#### 4.3.1. System performance during microwave treatment with bed fluidisation

The system's performance in terms of heating uniformity was evaluated by quantifying the Coefficient of Variation (CoV) of surface bed temperature measurements during heating tests using malted barley as the process material. This bed surface measurement is representative of particle surface temperatures in the bulk bed temperature thanks to the rapid particle movement and thorough mixing of the fluidisation regime of the reactor. Nine temperature measurement points distributed over a section of the bed observable by the thermal imaging camera were used to analyse heating uniformity, determining the CoV as the standard deviation over the mean of the temperature of these points.

A 500 mL sample of malted barley was charged to the reactor via the feeding port in the lid and fluidised at a fan speed of 1700 rpm for 15 s to achieve hydrodynamic steady state before microwave energy was applied. The thermal profile of the top surface of the fluidised bed was monitored using a FLIR e60 infrared thermal camera installed at a port in the lid of the reactor and connected to the FLIR Tools software. Tests were conducted at a gas temperature of 50 °C with no microwave power applied (conventional only mode) and then at a 50 °C gas temperature with both 2 and 4 kW of average absorbed power (hybrid mode). All the tests were conducted for 180 s. A schematic optical image of the observable section of the reactor taken from the Infrared imaging port is shown in Fig. 14, showing the selected measurement points.

In Fig. 15, example thermal images taken in the final second of each test can be seen, showcasing the temperature homogeneity.

Table 5 includes the average temperature reached for the toroidal bed of particles for each scenario. The surface bed temperature standard deviation is also shown as well as the CoV.

The calculated CoV quantifies the homogeneity of the heat treatment of the loaded bed of particles. This coefficient was found to be just ~1.6 % in both cases. When compared against conventional heating only, a significant reduction in the CoV is observed when combined with microwaves. Moreover, typical microwave heating processes have considerably higher CoV, even considering sophisticated uniformity improvement techniques [4,17,20,24,31–34,88]. This level of heating uniformity can be mainly attributed to the fast and thorough mixing and movement of the bed passing through the uniformly distributed microwave hotspots.

## 5. Thermodynamic characterisation

### 5.1. Experimental thermodynamic characterisation

Thermodynamic characterisation was carried out using the same four materials considered in the electromagnetic design of the system (malted barley, mung beans, yellow mustard seeds and green coffee beans). These particles were selected as a representative range of size and shape, with varying dielectric properties from moderate to moderately high loss. Their physical properties are shown in Table 6.

Thermal characterisation was carried out using 500 mL for each material and at two different temperatures, 50 and 100 °C, with average absorbed microwave power in the range 0 – 6 kW. Steady-state temperature was reached after ~200 s of microwave treatment for all samples. Averaged ΔT with absorbed microwave power at 200 s and is shown in Fig. 16.

A similar ΔT/kW is produced for all samples regardless of background air temperature. The microwave input power required to yield a given surface bed temperature was empirically derived, shown in Table 7.

Mean particle size range (2 – 2.5 mm to 8–9 mm) represented the operational window of the laboratory-scale Torwave® reactor in terms of effective toroidal fluidisation. Density and sphericity are broadly similar. Mung beans and mustard seeds presented a marginally more rounded morphology. In terms of response to microwave heating, given each feedstock type form a very similar bed cross-section and interaction volume, the dielectric properties of each feedstock are considered to be the dominant factor determining the power-temperature relationships presented in Table 7.

Overall, the system has been proven able to process a range of particles over a temperature range of 50 – 300 °C and microwave powers up to 6 kW with reliable performance, with bulk bed dielectric properties

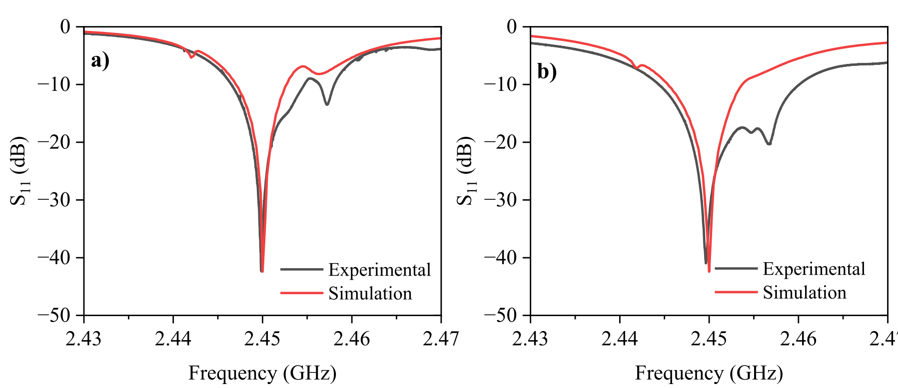


**Fig. 13.** Simulated (orange line) and measured S11 (blue line) reflection coefficient for moving beds of 500 mL (a) and 600 mL (b) of malted barley.

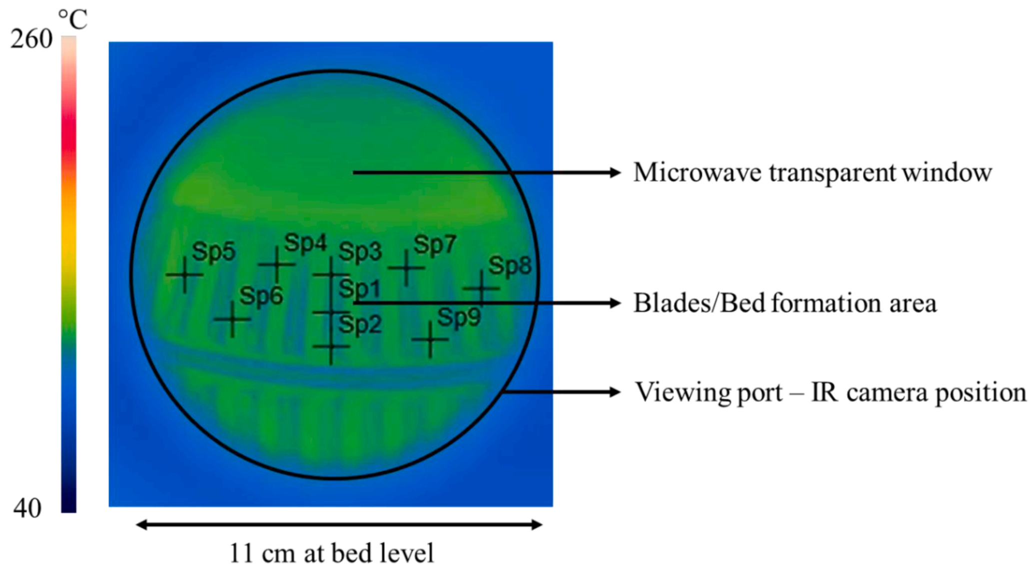


**Fig. 14.** Optical image taken from the IR port in the lid showing the observable section at the base of the empty reactor for reference against the thermal imaging tests.

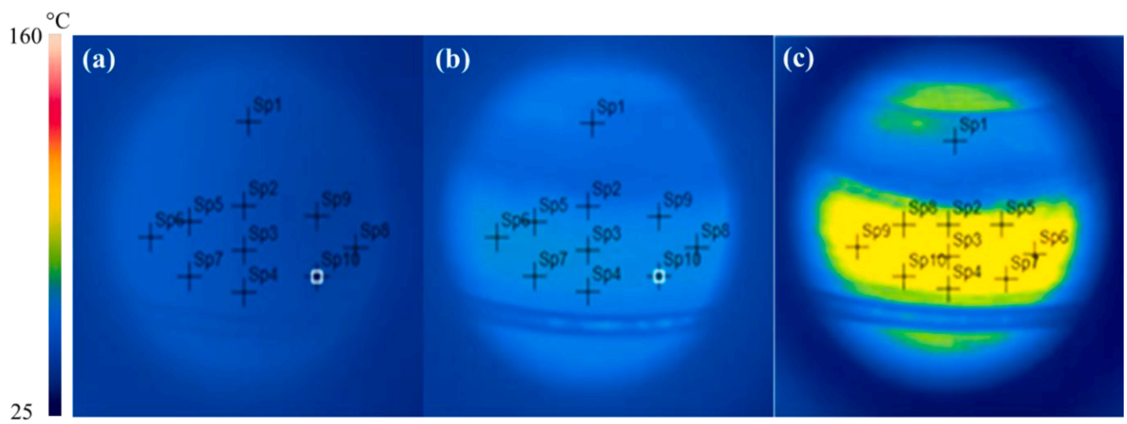


**Fig. 15.** Thermal images at the end of heating tests of malt for (a) conventional heating at 50 °C, (b) hybrid heating at 50 °C and 2 kW of average absorbed mw power, and (c) hybrid heating at 50 °C and 4 kW of average absorbed mw power.

**Table 5**
Summary of temperature results from malt heating tests using conventional only and two different hybrid operational modes at steady-state.

| Test | Conventional Only (a) | Hybrid (b) | Hybrid (c) |
|---|---|---|---|
| Average absorbed MW power (kW) | – | 2 | 4 |
| Average bed temperature achieved (°C) | 52.6 | 76.3 | 119.7 |
| Standard deviation | 4.1 | 1.2 | 1.9 |
| CoV (%) | 7.8 | 1.6 | 1.6 |

**Table 6**
Physical properties of the materials selected for the thermal characterisation.

| Particle | True Density (g/L) | Bulk density (g/L) | Size (mm) | Sphericity |
|---|---|---|---|---|
| Mustard seeds | 1105.0 ± 0.1 | 717.30 ± 2.03 | 2–2.5 | 0.87–0.89 |
| Mung Beans | 1386.6 ± 0.2 | 869.44 ± 2.68 | 5–6 | 0.84–0.86 |
| Malted Barley | 1461.1 ± 1.0 | 558.30 ± 3.26 | 8.5–9 | 0.53–0.55 |
| Green coffee beans | 1312.6 ± 0.4 | 617.85 ± 3.51 | 8–9 | 0.68–0.70 |

ranging from 1 to 4 dielectric constant and above 0.05 loss factor, although the system could be adjusted to operate in different ranges depending on the application. Residence time in the reactor will be dependant on the desired process outcome. For example, roasting applications are expected to require longer treatment times compared to drying or particle conditioning. The exploration of material-specific applications using the Torwave® system is ongoing, the outcomes of which are anticipated to be disseminated as part of future work.

## 6. Conclusions

A novel hybrid toroidal fluidised bed reactor combining convective and microwave heating has been developed. The applicator heating pattern was validated against electromagnetic simulations with good agreement using a foamed carbon as a proxy for a dynamic bed formed during toroidal fluidisation. Resonant characteristics showed only 1 MHz −10 dB bandwidth difference between experiments and simulations and were further validated dynamically using fluidised beds of malted barley, also showing good agreement. This underpins the use of the simulation methodology for fundamental system design.

The hydrodynamic characteristics of the reactor were evaluated for a range of particles. Optimal treatment volumes required for all the

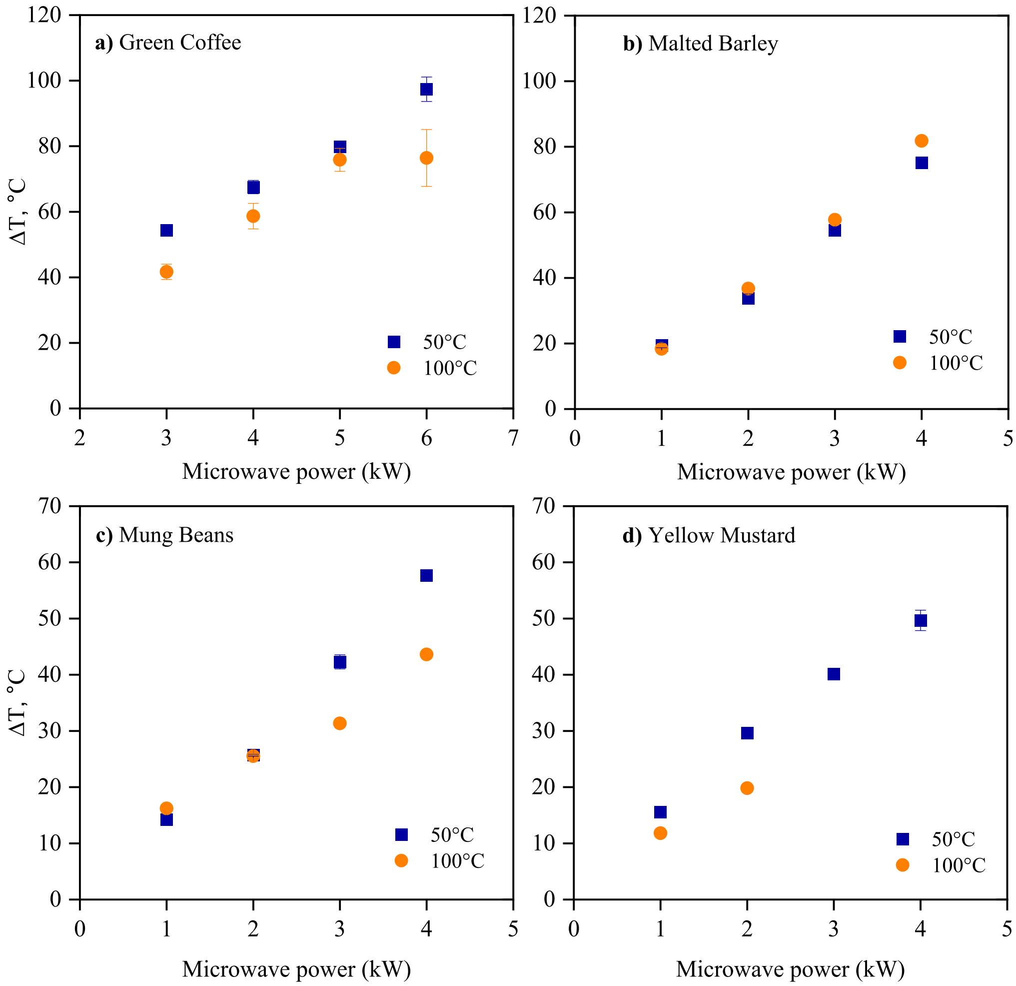


**Fig. 16.** Averaged ΔT after 200 s of treatment with MW Power for: Green coffee beans (a), Malted Barley (b), Mung Beans (c), and Yellow Mustard seeds (d) for 50 and 100 °C of background air temperature.

**Table 7**
Equations for the calculation of target surface bed temperature increment (ΔT) or absorbed microwave power (P) based on thermodynamic studies.

| Material | Equation |
|---|---|
| Green coffee beans | $\Delta T = 13.74\ P + 7.43$ |
| Malted barley | $\Delta T = 19.52$ P - 1.97 |
| Yellow mustard seeds | $\Delta T = 12.31\ P + 1.90$ |
| Mung beans | $\Delta T = 11.57\ P + 3.51$ |

particles to form the fluidised bed were found to be in the range of 400 – 600 mL and fluidisation velocity of 2.75 – 3.48 m/s. Using thermal imaging, the heating uniformity for an observable section of the fluidised bed was evaluated by taking temperature measurements at nine discrete points covering the observable area and width of the blade distributer. The system achieved an excellent level of treatment homogeneity using malted barley as a test feed with a Coefficient of Variation (CoV) of 1.6 % measured temperature across the bed surface at microwave powers of 2 and 4 kW respectively and gas temperature of 50 °C. This compares to a CoV of 7.8 % without microwave heating. Further experimental thermodynamic characterisation found that the input microwave power yielded a predictable increase in bed temperature, regardless of the temperature of the fluidisation gas. For malted barley, this resulted in an increase in bed temperature of 18.9 ± 0.9 °C/kW of absorbed microwave power.

The successful integration of the Torbed compact bed reactor and microwave applicator system has yielded an efficient, controllable system with the potential to be applied to particulate processing across a great number of sectors and industries, it could find industrial applications in sustainable processes, such as process intensification, carbon capture, torrefaction, exfoliation, roasting, sterilisation, expansion, drying, reduction, amongst many others. Future work involves specific process development, techno-economic and business case studies, and large-scale pilot trials.

## CRediT authorship contribution statement

**Jose Rodriguez:** Writing – review & editing, Writing – original draft, Visualization, Validation, Supervision, Project administration, Methodology, Investigation, Funding acquisition, Formal analysis, Data curation, Conceptualization. **Lorena Morona:** Visualization, Validation, Methodology, Investigation, Formal analysis, Data curation. **Maria Erans:** Writing – review & editing, Writing – original draft, Supervision, Project administration, Investigation. **Adam J. Buttress:** Writing – review & editing, Visualization, Project administration. **Matt Nicholls:** Visualization, Validation, Investigation. **Andrew R. Batchelor:** Writing – review & editing, Visualization, Project administration, Conceptualization. **Gabriela Duran-Jimenez:** Writing – review & editing, Visualization. **Sam Kingman:** Writing – review & editing, Supervision, Project administration, Funding acquisition, Conceptualization. **Daniel Groszek:** Writing – review & editing, Conceptualization. **Chris Dodds:**

Writing – review & editing, Supervision, Project administration, Funding acquisition, Conceptualization.

## Declaration of competing interest

The authors declare the following financial interests/personal relationships which may be considered as potential competing interests:

Jose Rodriguez reports financial support was provided by Agencia Nacional de Investigacion y Desarrollo de Chile (ANID). Chris Dodds reports financial support was provided by Innovate UK. Dan Groszek reports a relationship with Torftech Technologies Ltd. that includes: employment. Jose Rodriguez has patent #TOROIDAL PROCESSING CHAMBER (PCT/GB2022/052,624) pending to The University of Nottingham and Mortimer Technology Holdings Limited (part of the Torftech Group). Chris Dodds has patent #TOROIDAL PROCESSING CHAMBER (PCT/GB2022/052,624) pending to The University of Nottingham and Mortimer Technology Holdings Limited (part of the Torftech Group). Sam Kingman has patent #TOROIDAL PROCESSING CHAMBER (PCT/GB2022/052,624) pending to The University of Nottingham and Mortimer Technology Holdings Limited (part of the Torftech Group). If there are other authors, they declare that they have no known competing financial interests or personal relationships that could have appeared to influence the work reported in this paper.

## Data availability

Data will be made available on request.

## Acknowledgements

J.R. is grateful for funding from ANID Scholarship 21140769. This work was partially funded by UKRI through Innovate UK KTP011233 and received further support from the University of Nottingham EPSRC Impact Acceleration Account.

## References

[1] D. Beneroso, T. Monti, E.T. Kostas, J. Robinson, Microwave pyrolysis of biomass for bio-oil production: scalable processing concepts, Chem. Eng. J. 316 (2017) 481–498, https://doi.org/10.1016/j.cej.2017.01.130.
[2] E. Binner, E. Lester, S. Kingman, C. Dodds, J. Robinson, A Review of Microwave Coal Processing, J. Microwave Power Electromagn. Energy 48 (1) (2014) 35–60.
[3] K. Pitchai, S.L. Birla, J. Subbiah, D. Jones, H. Thippareddi, Coupled electromagnetic and heat transfer model for microwave heating in domestic ovens, J. Food Eng. 112 (1–2) (2012) 100–111, https://doi.org/10.1016/j.jfoodeng.2012.03.013.
[4] S.S.R. Geedipalli, V. Rakesh, A.K. Datta, Modeling the heating uniformity contributed by a rotating turntable in microwave ovens, J. Food Eng. 82 (3) (2007) 359–368, https://doi.org/10.1016/j.jfoodeng.2007.02.050.
[5] L. Shen, et al., Analysis of heating uniformity considering microwave transmission in stacked bulk of granular materials on a turntable in microwave ovens, J. Food Eng. 319 (2022) 110903, https://doi.org/10.1016/j.jfoodeng.2021.110903.
[6] J.L. Pedreño-Molina, J. Monzó-Cabrera, J.M. Catalá-Civera, Sample movement optimization for uniform heating in microwave heating ovens, Int. J. RF Microwave Comput. Aided Eng. 17 (2) (2007) 142–152, https://doi.org/10.1002/mmce.20208.
[7] A.J. Buttress, E. Binner, C. Yi, P. Palade, J.P. Robinson, S.W. Kingman, Development and evaluation of a continuous microwave processing system for hydrocarbon removal from solids, Chem. Eng. J. 283 (2016) 215–222, https://doi.org/10.1016/j.cej.2015.07.030.
[8] O. Udoudo, O. Folorunso, C. Dodds, S. Kingman, A. Ure, Understanding the performance of a pilot vermiculite exfoliation system through process mineralogy, Miner. Eng. 82 (2015) 84–91, https://doi.org/10.1016/j.mineng.2015.03.023.
[9] A.J. Buttress, et al., Towards large scale microwave treatment of ores: part 1 – Basis of design, construction and commissioning, Miner. Eng. 109 (2017) 169–183, https://doi.org/10.1016/j.mineng.2017.03.006.
[10] A.R. Batchelor, et al., Towards large scale microwave treatment of ores: part 2 – Metallurgical testing, Miner. Eng. 111 (2017) 5–24, https://doi.org/10.1016/j.mineng.2017.05.003.
[11] M. Adam, D. Beneroso, J. Katrib, S. Kingman, J.P. Robinson, Microwave fluidized bed for biomass pyrolysis. Part I: process design, Biofuels Bioprod. Biorefin. 11 (4) (2017) 601–612.
[12] M. Adam, D. Beneroso, J. Katrib, S. Kingman, J.P. Robinson, Microwave fluidized bed for biomass pyrolysis. Part II: effect of process parameters, Biofuels Bioprod. Biorefin. 11 (4) (2017) 613–624.
[13] M. Willert-Porada, A. Rosin, A. Schmidt, T. Gerdes, M. Adam, Analysis of microwave heating in a fluidized bed reactor, IEEE MTT-S International Microwave Symposium Digest (2014) 8–11, https://doi.org/10.1109/MWSYM.2014.6848517.
[14] M.H. Khoshtaghaza, H. Darvishi, S. Minaei, Effects of microwave - fluidized bed drying on quality, energy consumption and drying kinetics of soybean kernels, J. Food Sci. Technol. 52 (8) (2015) 4749–4760, https://doi.org/10.1007/s13197-014-1557-6.
[15] A.J. Buttress, et al., Design and optimisation of a microwave reactor for kilo-scale polymer synthesis, Chem. Eng. Sci.: X 2 (2019) 100022, https://doi.org/10.1016/j.cesx.2019.100022.
[16] H. Zhang, et al., Microwave pyrolysis of textile dyeing sludge in a continuously operated auger reactor, Fuel Process. Technol. 166 (2017) 174–185, https://doi.org/10.1016/j.fuproc.2017.05.031.
[17] F. Chen, A.D. Warning, A.K. Datta, X. Chen, Susceptors in microwave cavity heating: modeling and experimentation with a frozen pie, J. Food Eng. 195 (2017) 191–205, https://doi.org/10.1016/j.jfoodeng.2016.09.018.
[18] M. Bhattacharya, T. Basak, A review on the susceptor assisted microwave processing of materials, Energy 97 (2016) 306–338, https://doi.org/10.1016/j.energy.2015.11.034.
[19] B. Yahaya, S. Izman, M. Konneh, N. Redzuan, Microwave hybrid heating of materials using susceptors - A brief review, Adv Mat Res 845 (Dec. 2013) 426–430, https://doi.org/10.4028/www.scientific.net/AMR.845.426.
[20] S. Jeon, J. Kim, D. Yang, Design of large-scale microwave cavity for uniform and efficient plastic heating, Polymers (Basel) 14 (3) (2022) 541, https://doi.org/10.3390/polym14030541.
[21] L. Feher, M. Thumm, Microwave innovation for industrial composite fabrication—The HEPHAISTOS technology, IEEE Trans. Plasma Sci. 32 (1) (2004) 73–79, https://doi.org/10.1109/TPS.2004.823983.
[22] P. Plaza-González, J. Monzó-Cabrera, J.M. Catalá-Civera, D. Sánchez-Hernández, New approach for the prediction of the electric field distribution in multimode microwave-heating applicators with mode stirrers, IEEE Trans. Magn. 40 (3) (2004) 1672–1678, https://doi.org/10.1109/TMAG.2003.821560.
[23] V. Sebera, A. Nasswettrová, K. Nikl, Finite element analysis of mode stirrer impact on electric field uniformity in a microwave applicator, Drying Technol. 30 (13) (2012) 1388–1396, https://doi.org/10.1080/07373937.2012.664800.
[24] Y. Liao, et al., A phase-shifting method for improving the heating uniformity of microwave processing materials, Materials (Basel) 9 (5) (2016) 309, https://doi.org/10.3390/ma9050309.
[25] S.C. Kashyap, W. Wyslouzil, Methods for improving heating uniformity of microwave owens, J. Microwave Power 12 (3) (1977) 224–230, https://doi.org/10.1080/16070658.1977.11689050.
[26] J.R. Bows, M.L. Patrick, R. Janes, D.C. Dibben, Microwave phase control heating, Int. J. Food Sci. Technol. 34 (4) (1999) 295–304, https://doi.org/10.1046/j.1365-2621.1999.00272.x.
[27] H.S. Ku, F. Siu, E. Siores, J.A.R. Ball, A.S. Blicblau, Applications of fixed and variable frequency microwave (VFM) facilities in polymeric materials processing and joining, J. Mater. Process. Technol. 113 (1–3) (2001) 184–188, https://doi.org/10.1016/S0924-0136(01)00642-2.
[28] F. Yang, et al., Sweep frequency heating based on injection locked magnetron, Processes 7 (6) (2019), https://doi.org/10.3390/pr7060341.
[29] R. Yang, J. Chen, Heating performance of dual-source microwave heating using different frequency shifting strategies in a solid-state system, Food Res. Int. 175 (2024) 113781, https://doi.org/10.1016/j.foodres.2023.113781.
[30] E.D. Tortajada, P.P. Gonzalez, A.D. Morcillo, J.V. Balbastre, Optimisation of electric field uniformity in microwave heating systems by means of multi-feeding and genetic algorithms, Int. J. Mater. Prod. Technol. 29 (1/2/3/4) (2007) 149, https://doi.org/10.1504/IJMPT.2007.013134.
[31] J. Zhang, et al., Theoretical investigation of temperature distribution uniformity in wood during microwave drying in three-port feeding circular resonant cavity, Drying Technol. 35 (4) (2017) 409–416, https://doi.org/10.1080/07373937.2016.1178141.
[32] X. Li, Y. Luo, X. Li, J. Zhang, Theoretical study of wood microwave pretreatment in rectangular cavity for fabricating wood-based nanocomposites, J Nanomater 2014 (2014), https://doi.org/10.1155/2014/786312.
[33] Z. Zhang, T. Su, S. Zhang, Shape effect on the temperature field during microwave heating process, J. Food Qual. 2018 (2018) 1–24, https://doi.org/10.1155/2018/9169875.
[34] N. Soto-Reyes, A.L. Temis-Pérez, A. López-Malo, R. Rojas-Laguna, M.E. Sosa-Morales, Effects of shape and size of agar gels on heating uniformity during pulsed microwave treatment, J. Food Sci. 80 (5) (2015) E1021–E1025, https://doi.org/10.1111/1750-3841.12854.
[35] B.W. Raaholt, Influence of food geometry and dielectric properties on heating performance. Development of Packaging and Products for Use in Microwave Ovens, Elsevier, 2020, pp. 73–93, https://doi.org/10.1016/B978-0-08-102713-4.00002-5.
[36] A. Deng, X. Li, W. Qiu, L. Li, N. Tao, Y. Jin, Geometry optimization of microwavable food to improve heating uniformity, J. Food Eng. 369 (2024) 111945, https://doi.org/10.1016/j.jfoodeng.2024.111945.
[37] G. Brodie, The influence of load geometry on temperature distribution during microwave heating, Trans. ASABE 51 (4) (2008) 1401–1413, https://doi.org/10.13031/2013.25224.
[38] H. Kurniawan, S. Alapati, W.S. Che, Effect of mode stirrers in a multimode microwave-heating applicator with the conveyor belt, Int. J. Precision Eng.

Manufacturing - Green Technol. 2 (1) (2015) 31–36, https://doi.org/10.1007/s40684-015-0004-0.
[39] A.K. Datta, V. Rakesh, Principles of Microwave Combination Heating, Compr. Rev. Food Sci. Food Saf. 12 (1) (2013) 24–39, https://doi.org/10.1111/j.1541-4337.2012.00211.x.
[40] Z.Y. Li, R.F. Wang, T. Kudra, Uniformity Issue in Microwave Drying, Drying Technol. 29 (6) (2011) 652–660, https://doi.org/10.1080/07373937.2010.521963.
[41] K. Hara, M. Hayashi, Continuous Pig Iron Making by Microwave Heating with 12.5 kW at 2.45 GHz, J. Microwave Power Electromagn. Energy 45 (3) (2011) 137–147.
[42] K. Hara, M. Hayashi, M. Sato, K. Nagata, Pig Iron making by focused microwave beams with 20 kW at 2.45 GHz, ISIJ Int. 52 (12) (2012) 2149–2157, https://doi.org/10.2355/isijinternational.52.2149.
[43] M. Mehdizadeh, Microwave/RF Applicators and Probes, 2nd Editio, Elsevier, 2015.
[44] A. C, Metaxas, R.J. Meredith, Industrial Microwave Heating, IET, 1983.
[45] T.V.C.T. Chan, H.C. Reader, Understanding Microwave Heating Cavities, Artech House Publishers, 2000.
[46] K.M. Winter, J. Kalucki, D. Koshel, Process Technologies For Thermochemical Surface Engineering, Woodhead Publishing Limited, 2014, https://doi.org/10.1533/9780857096524.1.141.
[47] Torftech, Application Description - Vermiculite Exfoliation, 2015. Accessed: Feb. 21, 2024. [Online]. Available: http://www.torftech.com/pdf/Application%20Description%20-%20Vermiculite%20Exfoliation.pdf.
[48] A.V. Bridgwater, Review of fast pyrolysis of biomass and product upgrading, Biomass Bioenergy 38 (2012) 68–94, https://doi.org/10.1016/j.biombioe.2011.01.048.
[49] F.J. Smith, Microwave Fluidized Bed Dryer, 528, 1970, p. 179. US 3.
[50] J. Manser, G. Dankesreiter, Method and Apparatus For Bulk Material Treatment, 126, 1978, p. 945. US 4.
[51] Z.H. Wang, G. Chen, Theoretical study of fluidized-bed drying with microwave heating, Ind. Eng. Chem. Res. 39 (3) (2000) 775–782, https://doi.org/10.1021/ie990428a.
[52] A. Reyes, S. Cerón, R. Zúñiga, P. Moyano, A comparative study of microwave-assisted air drying of potato slices, Biosyst Eng 98 (3) (2007) 310–318, https://doi.org/10.1016/j.biosystemseng.2007.07.006.
[53] D. Zare, M. Ranjbaran, Simulation and validation of microwave-assisted fluidized bed drying of soybeans, Drying Technol. 30 (3) (2012) 236–247, https://doi.org/10.1080/07373937.2011.630765.
[54] G.R. Askari, Z. Emam-Djomeh, S.M. Mousavi, Heat and mass transfer in apple cubes in a microwave-assisted fluidized bed drier, Food Bioprod. Process. 91 (3) (2013) 207–215, https://doi.org/10.1016/j.fbp.2012.09.007.
[55] X. Hu, J. Kurian, Y. Gariepy, V. Raghavan, Optimization of microwave-assisted fluidized-bed drying of carrot slices, Drying Technol. 35 (10) (2017) 1234–1248, https://doi.org/10.1080/07373937.2016.1242014.
[56] I. Zahoor, et al., Microwave assisted fluidized bed drying of bitter gourd: modelling and optimization of process conditions based on bioactive components, Food Chem X 17 (2023) 100565, https://doi.org/10.1016/j.fochx.2023.100565.
[57] Y. Srinivas, S.M. Mathew, A. Kothakota, N. Sagarika, R. Pandiselvam, Microwave assisted fluidized bed drying of nutmeg mace for essential oil enriched extracts: an assessment of drying kinetics, process optimization and quality, Innovative Food Sci. Emerg. Technol. 66 (2020) 102541, https://doi.org/10.1016/j.ifset.2020.102541.
[58] A.G. Whittaker, D.M.P. Mingos, Microwave-assisted solid-state reactions involving metal powders and gases, J. Chem. Soc. Dalton Trans. (16) (1993) 2541, https://doi.org/10.1039/dt9930002541.
[59] J.M. Tranquilla, Method and Apparatus For Optimization of Energy Coupling For Microwave Treatment of Metal Ores and Concentrates in a Microwave Fluidized Bed Reactor, 074, 2000, p. 533. US 6.
[60] J. Tranquilla, Method and Apparatus For Microwaveinduced Pyrolysis of Arsenical Ores and Ore Concentrates, 2008. US 2008/0069746 A1.
[61] A.A. Salema, F.N. Ani, Microwave induced pyrolysis of oil palm biomass, Bioresour. Technol. 102 (3) (2011) 3388–3395, https://doi.org/10.1016/j.biortech.2010.09.115.
[62] M.A. Adam, Understanding Microwave Pyrolysis of Biomass Materials, University of Nottingham, 2017.
[63] E.P. Lynch, Use of Microwave Energy in Conjunction With Fluidized Bed Reactors, Argonne National Lab., Ill.(USA, 1977.
[64] H.Y. Kim, et al., Fluidized Bed Reactor Heated By Microwaves, 382, 1995, p. 412. US 5.
[65] M. Groszek and B. Laughllin, "Torbed Compact Bed Reactor (CBR)." Accessed: Feb. 21, 2024. [Online]. Available: http://www.torftech.com/pdf/CBR%20description.pdf.
[66] G.A. Wellwood, Hydrodynamic Behaviour of the Torbed(r) Reactor Operating in Fine Particle Mode, University of Queensland, 2000.
[67] M.F. B, V.R.R.K.V. Vinod, Study of the fluid dynamic performance of distributor type in torbed type reactors, Eng. e-Transaction 6 (1) (2011) 70–75.
[68] F.A.L. Dullien, Porous media: Fluid Transport and Pore Structure, Academic Press, 2012.
[69] J. Rodriguez, et al., S-band elliptical–cylindrical cavity resonator for material processing, Microw. Opt. Technol. Lett. 64 (12) (2022) 2160–2164, https://doi.org/10.1002/mop.33431.
[70] COMSOL Multiphysics(r) v. 6.2., "The RF Module User's Guide, 2023. Stockholm, Sweden[Online]. Available: www.comsol.com.
[71] C.A. Balanis, Advanced Engineering Electromagnetics, 2012.
[72] G. Tiwari, S. Wang, J. Tang, S.L. Birla, Analysis of radio frequency (RF) power distribution in dry food materials, J. Food Eng. 104 (4) (2011) 548–556, https://doi.org/10.1016/j.jfoodeng.2011.01.015.
[73] A. Porch, et al., Microwave treatment in oil refining, Appl Petrochem Res 2 (1–2) (2012) 37–44, https://doi.org/10.1007/s13203-012-0016-4.
[74] S. Ebadi, K. Forooraghi, An annular waveguide slot antenna, IEEE Antennas Wirel. Propag. Lett. 6 (1) (2007) 525–528, https://doi.org/10.1109/LAWP.2007.909966.
[75] C. William, et al., A Slotted-Waveguide Array For High-Power Microwave Transmission, 2001.
[76] T. Ha, R. Canfield, Design Optimization of a WR-90 Slotted Waveguide Antenna Stiffened Structures, in: 52nd AIAA/ASME/ASCE/AHS/ASC Structures, Structural Dynamics and Materials Conference April, 2011, pp. 1–12, https://doi.org/10.2514/6.2011-2147.
[77] A. Johannes, N. Maritz, Investigation and Design of a Slotted Waveguide Antenna with Low 3D by, 2010.
[78] H.M. El Misilmani, M. Al-husseini, K.Y. Kabalan, Design of slotted waveguide antennas with low sidelobes for high power microwave applications, Progress In Electromagnetics Research C 56 (January) (2015) 15–28.
[79] R.K. Enjiu, M.B. Perotoni, Slotted Waveguide Antenna Design Using 3D EM Simulation, 2013.
[80] R. Meredith, Engineer's Handbook of Industrial Microwave Heating, The Institution of Electrical Engineers, London, 1998.
[81] B.N. Das, J. Ramakrishna, B.K. Sarap, Resonant conductance of inclined slots in the narrow wall of a rectangular waveguide, IEEE Trans. Antennas Propag. 32 (7) (1984) 759–761, https://doi.org/10.1109/TAP.1984.1143401.
[82] A. Parkash, J.K. Vaid, A. Mansingh, Measurement of dielectric parameters at microwave frequencies by cavity-perturbation technique, IEEE Trans. Microw. Theory. Tech. 27 (9) (1979) 791–795, https://doi.org/10.1109/TMTT.1979.1129731.
[83] R.C. Jain, A proposed classification of dielectric materials on the basis of their losses in microwave frequency range, IETE Technical Review 15 (4) (1998) 291–295.
[84] R.S. Ferrari-John, et al., Electromagnetic heating for industrial kilning of malt: a feasibility study, Food. Bioproc. Tech. 10 (4) (2017) 687–698, https://doi.org/10.1007/s11947-016-1849-0.
[85] J. Baker-Jarvis, E.J. Vanzura, W.A. Kissick, Improved technique for determining complex permittivity with the transmission/reflection method, IEEE Trans. Microw. Theory. Tech. 38 (8) (1990) 1096–1103, https://doi.org/10.1109/22.57336.
[86] Daizo Kunii, Octave Levenspiel, Fluidization Engineering, 2nd, Butterworth-Heinemann, 1991.
[87] J. Katrib, O. Folorunso, C. Dodds, G. Dimitrakis, S.W. Kingman, Improving the design of industrial microwave processing systems through prediction of the dielectric properties of complex multi-layered materials, J. Mater. Sci. 50 (23) (2015) 7591–7599, https://doi.org/10.1007/s10853-015-9319-z.
[88] V. Rakesh, A.K. Datta, M.H.G. Amin, L.D. Hall, Heating uniformity and rates in a domestic microwave combination oven, J. Food Process Eng. 32 (3) (2009) 398–424, https://doi.org/10.1111/j.1745-4530.2007.00224.x.